A&A 598, A62 (2017)
DOI: 10.1051/0004-6361/201629494

Astronomy & Astrophysics

Dipole modes with depressed amplitudes in red giants are mixed modes

B. Mosser[1], K. Belkacem[1], C. Pinçon[1], M. Takata[2], M. Vrard[3], C. Barban[1], M.-J. Goupil[1], T. Kallinger[4], and R. Samadi[1]

[1] LESIA, Observatoire de Paris, PSL Research University, CNRS, Université Pierre et Marie Curie, Université Paris Diderot, 92195 Meudon, France
e-mail: benoit.mosser@obspm.fr
[2] Department of Astronomy, School of Science, The University of Tokyo, 7-3-1 Hongo, Bunkyo-ku, Tokyo 113-0033, Japan
[3] Instituto de Astrofísica e Ciências do Espaço, Universidade do Porto, CAUP, Rua das Estrelas, 4150-762 Porto, Portugal
[4] Institute of Astrophysics, University of Vienna, Türkenschanzstrasse 17, 1180 Vienna, Austria

Received 5 August 2016 / Accepted 11 October 2016

ABSTRACT

Context. Seismic observations with the space-borne *Kepler* mission have shown that a number of evolved stars exhibit low-amplitude dipole modes, which is referred to as depressed modes. Recently, these low amplitudes have been attributed to the presence of a strong magnetic field in the stellar core of those stars. Subsequently, and based on this scenario, the prevalence of high magnetic fields in evolved stars has been inferred. It should be noted, however, that this conclusion remains indirect.
Aims. We intend to study the properties of mode depression in evolved stars, which is a necessary condition before reaching conclusions about the physical nature of the mechanism responsible for the reduction of the dipole mode amplitudes.
Methods. We perform a thorough characterization of the global seismic parameters of depressed dipole modes and show that these modes have a mixed character. The observation of stars showing dipole mixed modes that are depressed is especially useful for deriving model-independent conclusions on the dipole mode damping. We use a simple model to explain how mode visibilities are connected to the extra damping seen in depressed modes.
Results. Observations prove that depressed dipole modes in red giants are not pure pressure modes but mixed modes. This result, observed in more than 90% of the bright stars ($m_V \leq 11$), invalidates the hypothesis that depressed dipole modes result from the suppression of the oscillation in the radiative core of the stars. Observations also show that, except for visibility, seismic properties of the stars with depressed modes are equivalent to those of normal stars. The measurement of the extra damping that is responsible for the reduction of mode amplitudes, without any prior on its physical nature, potentially provides an efficient tool for elucidating the mechanism responsible for the mode depression.
Conclusions. The mixed nature of the depressed modes in red giants and their unperturbed global seismic parameters carry strong constraints on the physical mechanism responsible for the damping of the oscillation in the core. This mechanism is able to damp the oscillation in the core but cannot fully suppress it. Moreover, it cannot modify the radiative cavity probed by the gravity component of the mixed modes. The recent mechanism involving high magnetic fields proposed for explaining depressed modes is not compliant with the observations and cannot be used to infer the strength and prevalence of high magnetic fields in red giants.

Key words. stars: oscillations – stars: evolution – stars: magnetic field – stars: interiors

1. Introduction

Asteroseismic observations by the CoRoT and *Kepler* space-borne missions have provided new insights in stellar and Galactic physics (e.g., Michel et al. 2008; Miglio et al. 2009; Chaplin et al. 2011). The ability to derive fundamental stellar parameters, such as masses and radii, over a wide range of stellar evolutionary states from the main sequence to the asymptotic giant branch is certainly one of the strongest impacts of such measurements (e.g., Kallinger et al. 2010). The rich nature of the red giant oscillation spectrum was largely unexpected (De Ridder et al. 2009; Mosser & Miglio 2016). Red giant asteroseismology has been boosted by the observation of dipole modes that, because of their mixed nature, probe the stellar core. They behave as gravity modes in the core and as pressure modes in the envelope. The pressure components carry information on the mass and radius of stars (e.g., Mosser et al. 2013), while the gravity components of these mixed modes are directly sensitive to the size and mass of the helium core (Montalbán & Noels 2013; Lagarde et al. 2016); to the evolutionary stage, which differs according to the nuclear reaction at work (Bedding et al. 2011; Mosser et al. 2011); and to the mean core rotation (Beck et al. 2012; Mosser et al. 2012b; Deheuvels et al. 2012, 2014).

Because of the homology of the red giant interior structure, red giant seismology is characterized by the many scaling relations between global seismic parameters along stellar evolution (e.g., Stello et al. 2009; Mosser et al. 2010; Mathur et al. 2011; Kallinger et al. 2012). Exceptions to these relations are rare and most often explained by specific features, such as for instance the damping of the oscillation in close binaries (Gaulme et al. 2014) or very low metallicity (Epstein et al. 2014). However, observations have revealed that a family of red giants exhibit peculiar dipole modes with low amplitudes (Mosser et al. 2012a). In some extreme cases, dipole modes are not even detectable.

Consequently, these dipole modes have been called depressed modes[1].

The first in-depth study of a star with depressed modes could not explain this phenomenon (García et al. 2014). Then, Fuller et al. (2015) addressed this issue by using a twofold approach. First, the authors expressed the dipole mode visibilities in the limit of full suppression of the oscillation in the red giant core. In other words, they assumed that the mode energy that leaks in the radiative interior of red giants is totally lost. As a consequence, dipole modes are no longer mixed modes but only lie in the upper (acoustic) cavity of red giants. This assumption is validated by the authors by means of a comparison between observed and computed mode visibilities. Second, it is conjectured that the extra loss of the mode energy is caused by a strong magnetic field, which scatters waves leaking in the core. This prevents these waves from constructing a standing wave in the inner resonant cavity of those stars. This has been named the magnetic greenhouse effect. The angular degree dependence of the energy leakage has been verified with the quadrupole modes (Stello et al. 2016a). This appealing scenario has then been taken for granted by Stello et al. (2016b) and Cantiello et al. (2016) to infer the prevalence of magnetic fields in the core of oscillating red giant stars observed by *Kepler*.

However, before firmly concluding about the presence of a magnetic field in the core of red giants with depressed modes, the hypothesis of the suppression of the oscillation in the core has to be validated. In fact, the nature of the physical mechanism responsible for the reduction of dipole mode visibilities is not directly inferred by the observation of low mode visibilities. Therefore, the identification of a magnetic field as the physical mechanism responsible for the suppression of the oscillation in the core of those stars demands further direct observational confirmation. A strong magnetic field is a possible solution, but it is not the only solution. Fuller et al. (2015) note that rapid core rotation should have the same effect, but would require much larger rotation rates than observed in red giants (Mosser et al. 2012b; Deheuvels et al. 2014). Indeed, any strong damping in the core, such as radiative damping or gravity wave reflection that is caused, for instance, by a steep composition gradient above the hydrogen burning shell, could also explain the depressed modes (Dziembowski 2012).

In this work, we aim to provide a complete characterization of the population of red giants with depressed modes using *Kepler* observations. This study is motivated by the observation of stars showing dipole modes that are both mixed and depressed. We argue that the full characterization of stars with depressed visibilities can provide strong constraints on the physical mechanism responsible for the damping of the oscillation.

The article is organized as follows. Section 2 presents the theoretical background of mode visibility with an emphasis on the distinction between full and partial mode damping in the core of red giants. In Sect. 3, we undertake the characterization of depressed modes with a mixed character, hereafter named depressed mixed modes. We first explain how they were identified, then exploit their observations with the determination of their global seismic properties. We also consider stars where, owing to the too low visibility of dipole modes, the gravity-dominated mixed modes are apparently absent. Global properties of stars are then used to test the depressed visibilities predicted when the oscillation is suppressed in the stellar core (Sect. 4). Section 5 is devoted to discussion with particular attention to the nature of the mechanism responsible for the extra damping of depressed modes. Finally, Sect. 6 is dedicated to conclusions.

[1] In the following, we use the term depressed for modes exhibiting diminished visibilities and keep the term suppressed for the suppression of the oscillation in the stellar core. As shown in Sect. 2.3, the full suppression of the oscillation in the core induces the mode depression. In contrast, normal modes have normal visibilities. Suppression implicitly means full suppression, so that we introduce the term partial suppression when we have to stress that the supposed suppression is not total. We do not use the term mode suppression, since it can only correspond to a null visibility.

2. Dipole mode visibilities

2.1. General case

The mode visibility is a way to express the mean value of the squared amplitude of modes with a given degree compared to radial modes. For a dipole mode, we define

$$V_1^2 = \frac{A_1^2}{A_0^2}\,\tilde{V}_1^2, \tag{1}$$

where $\tilde{V}_1^2$ includes the contributions of several physical effects: a geometrical factor that depends on the angular degree, limb darkening, and bolometric correction. The values A_0 and A_1 are the intrinsic amplitudes of the radial and dipole modes, respectively. For stars exhibiting stochastically excited pure acoustic modes, these amplitudes are supposed to be equal (Belkacem et al. 2008). In such a case, the visibility V_1^2 reduces to $\tilde{V}_1^2$.

A simple way to address the depressed modes consists in normalizing the dipole visibility with respect to the nominal expected value. We therefore use the same definition as Fuller et al. (2015) for expressing the relative visibility of depressed modes. In a first step, we consider the individual visibilities of the mixed modes,

$$v_{n_\mathrm{m}} = \frac{V_{1\,\mathrm{depressed}}^2}{\tilde{V}_1^2}, \tag{2}$$

where the mixed order n_m labels the mixed mode (Eqs. (4.60)–(4.63) of Mosser 2015). Strictly speaking, v_{n_m} should be referred to as a ratio of the squared amplitudes of dipole modes compared to radial modes, since the contribution of the different visibility terms (aspect ratio of the spherical harmonics and limb-darkening coefficients) is removed by the ratio to $\tilde{V}_1^2$. However, we keep the term visibility for the sake of simplicity.

For red giants, Ballot et al. (2011) computed $\tilde{V}_1^2 \simeq 1.54$, assuming that only acoustic modes are present. In evolved stars, the situation is in fact complicated by mixed modes. The contribution of all mixed modes associated with a given pressure radial order n_p can be expressed as

$$v = \sum_{n_\mathrm{m}\in\{\mathcal{N}\}} v_{n_\mathrm{m}}. \tag{3}$$

The sum is made in the ensemble $\{\mathcal{N}\}$ of the $\mathcal{N}$ mixed modes associated with a given pressure radial order. They lie in the $\Delta\nu$-wide frequency range between two radial modes: for the pressure radial order around ν_max, $\mathcal{N} = \Delta\nu\Delta\Pi_1^{-1}\nu_\mathrm{max}^{-2}$, where $\Delta\nu$ is the mean large separation of pressure modes, $\Delta\Pi_1$ is the period spacing of gravity modes, and ν_max is the frequency of maximum oscillation signal.

The mixed-mode visibility v_{n_m} introduced by Eq. (2) has been investigated in previous work (Dupret et al. 2009; Benomar et al. 2014; Grosjean et al. 2014), which shows

$$v_{n_\mathrm{m}} \simeq \left(\frac{\Gamma_0}{\Gamma_{n_\mathrm{m}}}\right)\left(\frac{I_0}{I_{n_\mathrm{m}}}\right)^2, \tag{4}$$

where Γ_0, Γ_{n_m} (I_0, I_{n_m}) are the line widths (inertia) of the radial and dipole modes, respectively. This equation is valid whether the dipole mode is resolved or not, but assumes that the driving is the same for radial and dipole modes. To go further, we have to examine two cases, depending on the assumption on the dipole modes.

2.2. Normal dipole mixed modes

Following Belkacem et al. (2015), we may consider that the work performed by the gas during one oscillation cycle, associated with surface damping, is the same for all modes, so that Eq. (4) is simplified into

$$v_{n_m} \simeq \frac{I_0}{I_{n_m}} \simeq \frac{\Gamma_{n_m}}{\Gamma_0}, \tag{5}$$

from which we retrieve that the individual visibilities of mixed modes are small with smaller mode widths and larger inertia than radial modes.

From observations, Mosser et al. (2012a) have shown that the contribution of all mixed modes associated with a given pressure radial order n_p ensures $v = 1$. Here, we can demonstrate this, using the relation between inertia and the function ζ that governs the mixed-mode spacings and the rotational splittings (Goupil et al. 2013; Deheuvels et al. 2015; Mosser et al. 2015). From $I_0/I_{n_m} = 1 - \zeta$, we have

$$v = \sum_{n_m \in \{\mathcal{N}\}} (1 - \zeta). \tag{6}$$

The $\mathcal{N}$ mixed modes in the ensemble $\{\mathcal{N}\}$ between two consecutive radial modes correspond to 1 pure pressure dipole mode and $(\mathcal{N} - 1)$ pure gravity dipole modes. The period difference between the two radial modes can be estimated in two ways as follows: either considering the sum $(\mathcal{N}-1)\,\Delta\Pi_1$ for the pure gravity modes or considering the sum of the mixed-mode period spacings, $\sum_{n_m \in \{\mathcal{N}\}} \Delta P = (\sum_{n_m \in \{\mathcal{N}\}} \zeta)\ \Delta\Pi_1$, according to Mosser et al. (2015). Hence, we get

$$v = \sum_{n_m \in \{\mathcal{N}\}} (1 - \zeta) = \mathcal{N} - (\mathcal{N} - 1) = 1. \tag{7}$$

This result proves that, despite the mixed nature of the dipole modes, their total visibility matches the expected visibility of the corresponding pure pressure mode. So, energy equipartition is preserved for the normal mixed modes.

2.3. A particular case: suppression of the oscillation in the core

The possibility of suppression of the oscillation in the core was first investigated by Unno et al. (1989). Their Eqs. (16.62)–(16.65) consider the effect of a wave leakage in the core of an acoustic mode trapped in the convective envelope. The limit of oscillation suppression in the core implies that only pressure dipole modes are present since mixed modes are necessarily canceled out. In that case, $I_1 \simeq I_0$, so that Eq. (4) is rewritten as

$$v = \frac{\Gamma_0}{\Gamma_1}. \tag{8}$$

The damping in the core, whatever it is, can be written

$$v = \frac{\Gamma_0}{\Gamma_1^{\rm env} + \Gamma_1^{\rm core}} \simeq \frac{\Gamma_0}{\Gamma_0 + \Gamma_1^{\rm core}}, \tag{9}$$

where $\Gamma_1^{\rm env} \simeq \Gamma_0$ and $\Gamma_1^{\rm core}$ are the damping contributions in the envelope and in the core, respectively.

2.3.1. Damping and transmission

Equation (9) can be rewritten

$$v = \frac{1}{1 + x} \quad \text{with} \quad x = \frac{\Gamma_1^{\rm core}}{\Gamma_0}. \tag{10}$$

When all energy transmitted in the core is absorbed or damped, following Unno et al. (1989) we get

$$x = \omega\tau_{\rm a} \left(\int_{\mathcal{A}} k_r \, {\rm d}r \right)^{-1} \frac{1}{4} \exp\left(-2 \int_{\mathcal{E}} \kappa \, {\rm d}r \right), \tag{11}$$

where $\mathcal{A}$ denotes integration in the acoustic cavity and $\mathcal{E}$ in the evanescent region, k_r is the radial wave number, $\kappa^2 = -k_r^2$, ω is the mode frequency, and $\tau_{\rm a}$ is the e-folding damping time of the radial mode amplitude. At first order, the first integral of Eq. (11) equals $\omega/2\Delta\nu$, where $\Delta\nu$ is the large separation. Thus, Eq. (11) becomes

$$x = \frac{\Delta\nu\,\tau_{\rm a}}{2} \exp\left(-2 \int_{\mathcal{E}} \kappa {\rm d}r \right). \tag{12}$$

We then introduce the e-folding damping time of the mode energy, $\tau_0 = \tau_{\rm a}/2$ and get

$$v = \left(1 + \Delta\nu\,\tau_0\,T^2 \right)^{-1}, \tag{13}$$

where the transmission in the evanescent region is defined by

$$T = \exp\left(- \int_{\mathcal{E}} \kappa {\rm d}r \right). \tag{14}$$

Equation (13), derived from the relative visibility of depressed dipole modes with respect to radial modes, is similar to Eq. (2) of Fuller et al. (2015), which is derived from the ratio between the depressed and normal dipole modes.

2.3.2. Link with observable parameters

We can match the value of T^2 with the coupling factor q of mixed modes (Unno et al. 1989),

$$T^2 = 4q. \tag{15}$$

The visibility can thus be expressed as a function of the seismic observables q and Γ_0

$$v = \left(1 + 2q\,\frac{\Delta\nu}{\pi\Gamma_0} \right)^{-1}. \tag{16}$$

The coupling factor q is obtained from the asymptotic expansion of mixed modes

$$\tan\theta_{\rm p} = q \tan\theta_{\rm g}, \tag{17}$$

where the phases $\theta_{\rm p}$ and $\theta_{\rm g}$ refer, respectively, to the pressure- and gravity-wave contributions (Mosser et al. 2015). The radial mode width Γ_0, which is measured as the full width at half maximum in the power density spectrum, is related to the radial mode lifetime by (see Samadi et al. 2015)

$$\Gamma_0 = \frac{1}{2\pi\tau_0}. \tag{18}$$

In fact, Eqs. (15) and (16) are no longer valid when the extent of the evanescent region is limited, so that strong coupling occurs. In that case (see Takata 2016a),

$$T^2 = \frac{4q}{(1+q)^2}. \tag{19}$$

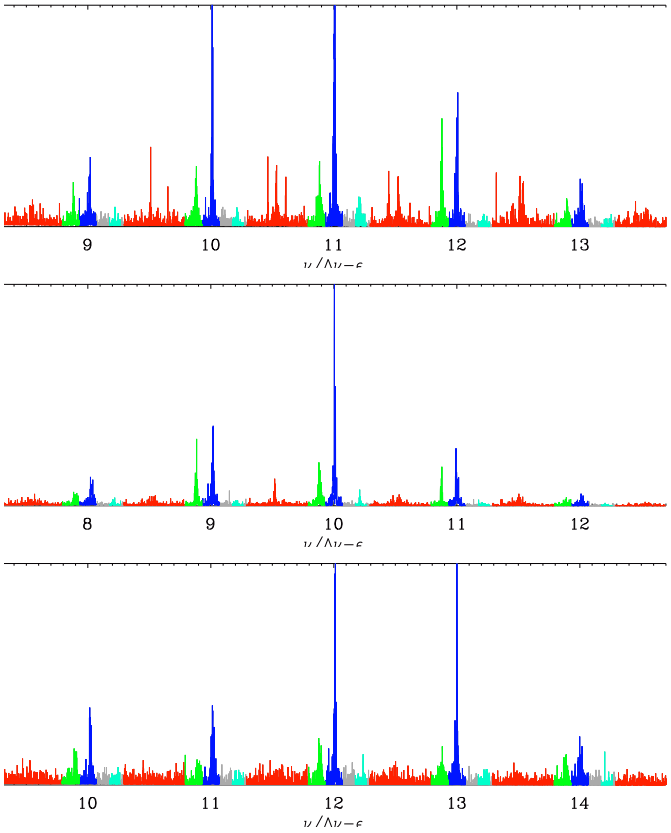

Fig. 1. Examples of red giant branch stars with low dipole-mode amplitudes. Spectra are plotted as a function of the reduced frequency $\nu/\Delta\nu - \varepsilon$, so that radial modes (shown in blue) are close to integer values; quadrupole modes are plotted in green, octupole modes in cyan; and mixed modes can be found everywhere but their contribution is measured in the frequency range plotted in red only. The mean background component was subtracted. *Top*: the mixed mode pattern of KIC 9279486 can be fitted to extract seismic global parameters; *middle*: the mixed modes in KIC 6026983 are evidenced but their pattern cannot be fit; and *bottom*: the dipole modes of KIC 5810513 have very small amplitudes but can be unambiguously detected and identified as mixed modes with the method discussed in Sect. 3.3.

Following Eq. (71) of Takata (2016b), we also have to replace T^2 by $-\ln(1-T^2)$ in case of full suppression of the oscillation in the core. So, Eq. (13) becomes

$$v = \left(1 - \ln\left[1 - \frac{4\,q}{(1+q)^2}\right]\frac{\Delta\nu}{2\pi\Gamma_0}\right)^{-1}. \tag{20}$$

Contrary to Eq. (13), this expression ensures a null visibility in case of total transmission ($T = q = 1$).

3. Seismic observables

Previous observations have reported that the depressed modes in the red giant KIC 8561221 are mixed (García et al. 2014). Such observations question the hypothesis of oscillation suppression: if the low visibility derives from the suppression of the oscillation in the radiative core, mixed modes cannot be established. Therefore, we first aim to identify the prevalence of red giants with depressed mixed modes. Then, we also use different observations to assess the properties of depressed dipole modes to determine whether they are mixed or not. Figure 1 illustrates the different types of stars we intend to work with: either

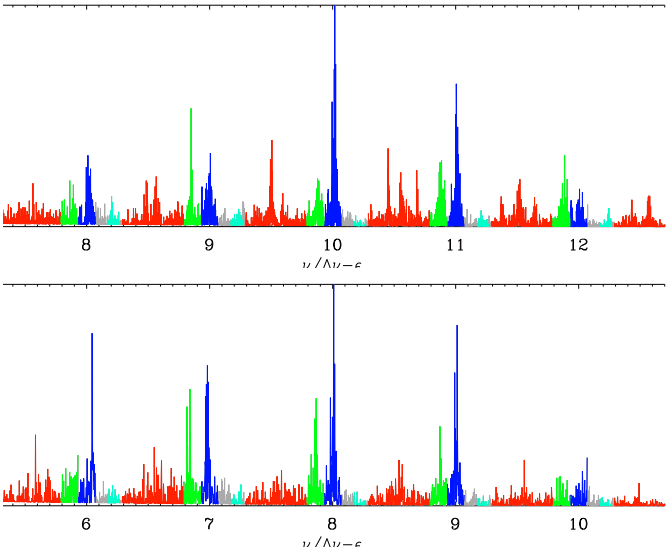

Fig. 2. Same as Fig. 1 but for core-helium burning stars. *Top*: the mixed mode pattern of the secondary-clump star KIC 8522050 can be fitted to extract seismic global parameters; and *bottom*: the depressed mixed modes in the clump star KIC 2693261 are apparent but their pattern cannot be fit.

with depressed mixed modes that can be identified, depressed mixed modes that cannot be fitted, or without clear evidence of mixed modes. Figure 2 provides examples for core-helium burning stars.

3.1. Identification of low visibilities

The first step for the search of stars with dipole mixed modes consists in the measurement of reduced visibilities, as defined by Eq. (3), with the method of Mosser et al. (2012a). In short, squared amplitudes are estimated from the integration of the power spectrum density over the frequency range covering the different modes, after subtraction of background. We obtained the total dipole visibilities, V_1^2, for about 12 500 red giants of the *Kepler* public data (Fig. 3a), from which we could identify the population of stars on the red giant branch (RGB) with normal visibilities and the family of stars with low visibility, in agreement with Mosser et al. (2012a) and Stello et al. (2016a). Red giants with normal amplitudes have a total dipole visibility of close to $\tilde{V}_1^2 \simeq 1.54$ with a very weak dependence on $T_{\rm eff}$, $\log g$, and Z. Using effective temperatures of Huber et al. (2014), we found that the normal (not depressed) visibilities of red giants, integrated for one pressure radial order, follow the mean trend

$$\langle \tilde{V}_1^2 \rangle \simeq 1.54 - \frac{T_{\rm eff} - 4850}{4100}, \tag{21}$$

where the brackets indicate the average value derived from a linear fit with the effective temperature $T_{\rm eff}$ expressed in kelvin. This result is very close to the predictions of Ballot et al. (2011).

The mean value of the normal visibility was then used to derive reduced integrated observed visibilities,

$$v_1 = \frac{\overline{\sum V_1^2}}{\langle \tilde{V}_1^2 \rangle}, \tag{22}$$

where, for the numerator, the sum matches all dipole modes associated with a given pressure radial order and the overbar represents the mean value for the different radial orders where dipole

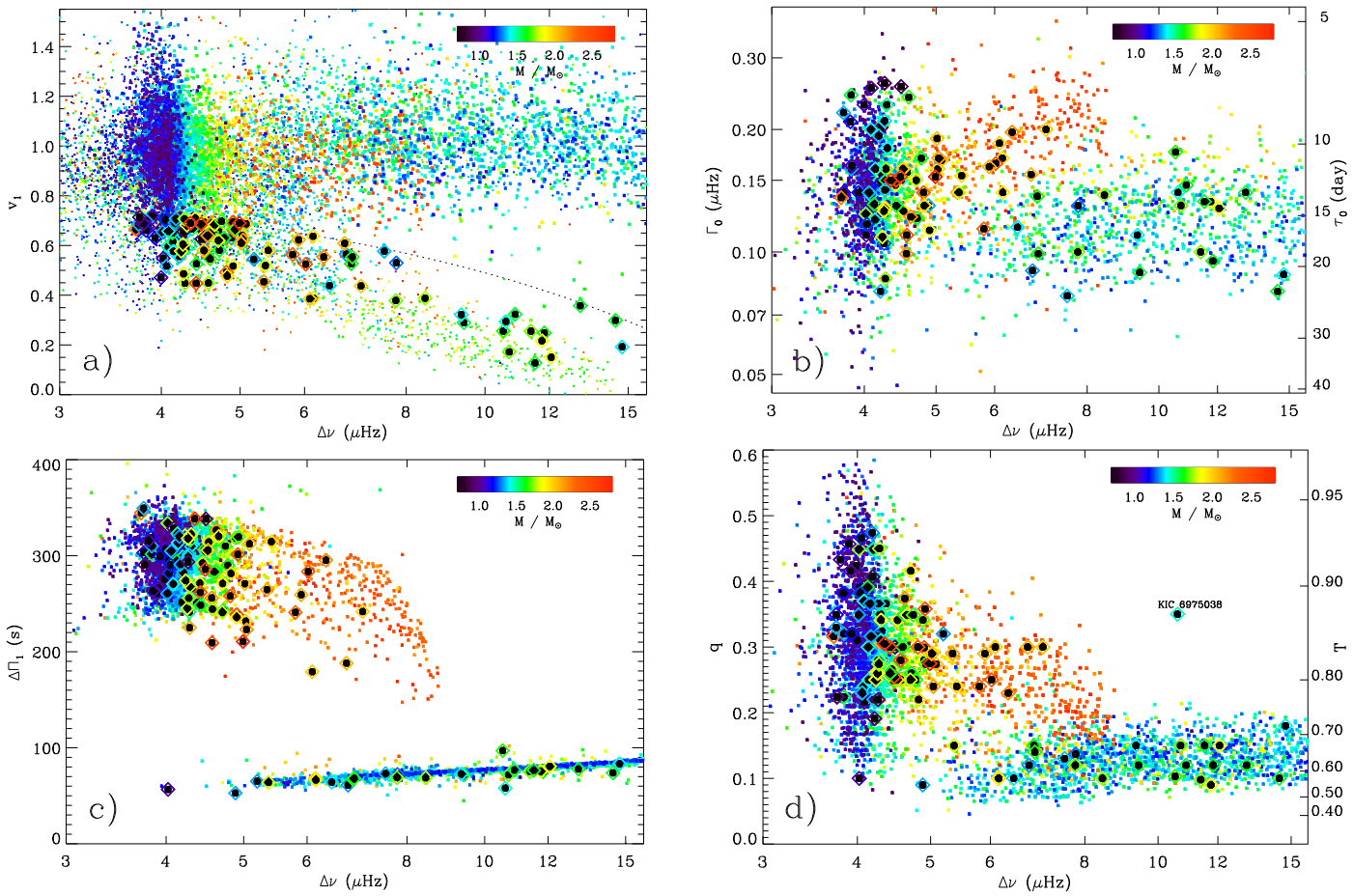

Fig. 3. a) Dipole mode visibility v_1 as a function of the large separation $\Delta\nu$. The color codes the mass determined with seismic scaling relations. Small symbols represent *Kepler* stars of the public data set; and larger symbols represent stars of the data set studied by Vrard et al. (2016). Diamonds with a dark center are stars showing depressed mixed modes. The dashed line represents the limit defining low visibilities. **b)** Radial mode width Γ_0 as a function of the large separation $\Delta\nu$ of the data set studied by Vrard et al. (2016). The right y-axis provides the radial mode lifetime. **c)** Same as **b)** for the period spacings $\Delta\Pi_1$; and **d)** same as **b)** for the coupling factor q. The outlying value of q for KIC 6975038 is discussed in Sect. 5.4.

modes are observed. Now, v_1 can be compared to v (Eq. (3)). As stated by previous work, the limit between normal and low visibility is clear on the RGB, despite the presence of a few stars lying in the no man's land between normal and reduced visibilities; in the red clump, we chose to define low-visibility stars by $v_1 \leq 0.85 - 0.04\,\Delta\nu$ (with $\Delta\nu$ expressed in μHz). We tested that changing the threshold value does not significantly change the conclusions of the work.

3.2. Fit of the mixed-mode pattern

The systematic search for stars with depressed mixed modes was derived from the recent work of Vrard et al. (2016), who have measured the asymptotic period spacing of mixed modes for about 6100 red giants. We then fitted the asymptotic mixed-mode pattern in stars with reduced dipole visibilities.

The fit of mixed mode frequencies in red giants is usually made easy by the use of asymptotic expansion (Unno et al. 1989; Mosser et al. 2012b), but is more difficult in stars with depressed mixed modes because of the lower signal-to-noise ratio induced by low visibilities. However, we managed to optimize this fitting process to obtain complete sets of seismic parameters, including rotational splittings $\delta\nu_{\rm rot}$ (Mosser et al. 2012b). Recent methods and results based on four years of *Kepler* observation were used to update previous measurements (Mosser et al. 2014, 2015; Vrard et al. 2016). Stellar masses were estimated from the seismic scaling relation with the method of Mosser et al. (2013) to have a better calibration than the solar calibration and to lower the non-negligible noise induced by pressure glitches (Vrard et al. 2015). Scaling relations have been used with the effective temperature of Huber et al. (2014).

We were able to fit the asymptotic mixed-mode pattern, including the rotational splittings, for 71 red giants (Table A.1, Fig. 4). This number represents a small fraction of the 1109 stars with low amplitudes since fitting all parameters of the asymptotic mixed-mode pattern is highly demanding when amplitudes are depressed. Unsurprisingly, owing to the aforementioned observational bias, our data set with mixed modes on the RGB is biased toward high visibilities (Fig. 3a). Conversely, as low visibilities of clump stars are not as low as they are on the RGB, fitting their mixed modes is easier. With this analysis, we can establish the properties of stars with depressed mixed modes.

Mass. Stars in our data set with depressed mixed modes present larger masses than the typical mass distribution of CoRoT or *Kepler* red giants showing solar-like oscillations. Their median mass is $1.6\,M_\odot$, which is above the median mass of the red

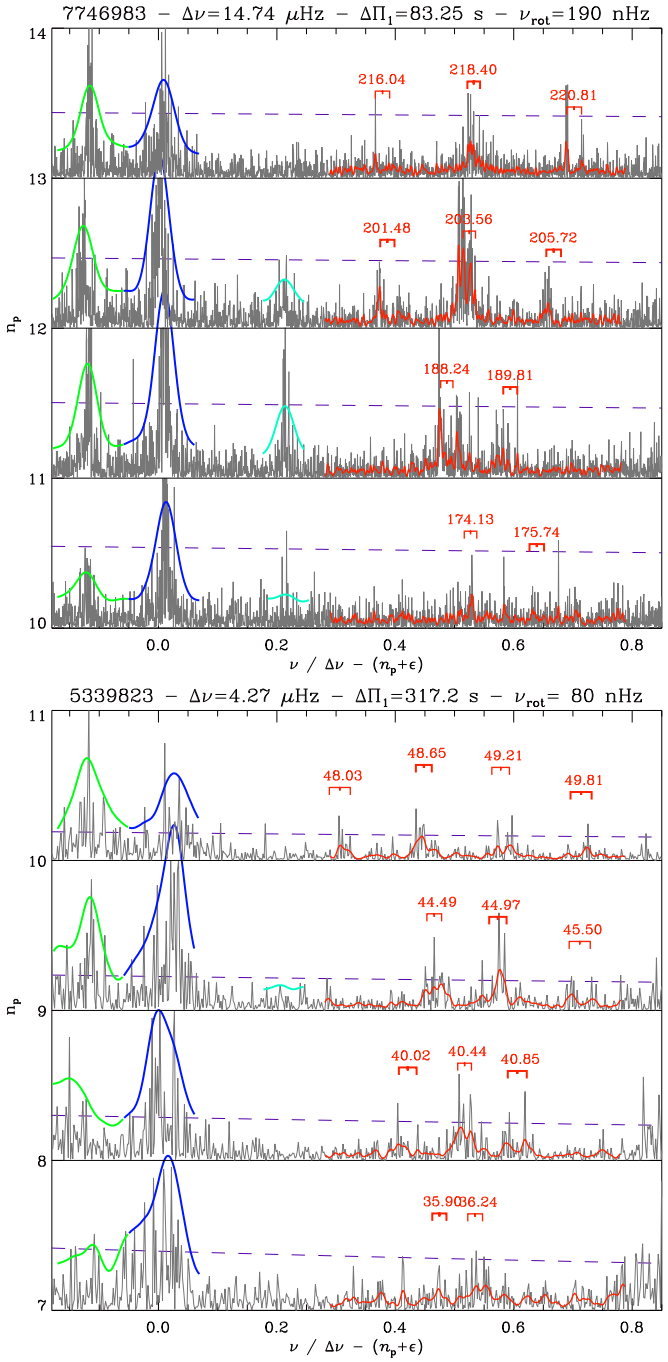

Fig. 4. Examples of complete fits of the asymptotic mixed-mode pattern of red giants with low dipole-mode amplitudes. Échelle diagrams are plotted as a function of the reduced frequency $\nu/\Delta\nu - (n_p + \varepsilon)$, so that radial modes are close to integer values. The smoothed profile of mixed modes are plotted in red, quadrupole modes in green, and octupole modes in cyan. The dashed gray line corresponds to 8 times the granulation background. Dipole triplets are identified by the asymptotic cyclic frequency, in μHz, of the $m = 0$ component. *Top*: RGB star, KIC 7746983; *bottom*: Clump star, KIC 5339823.

giants observed with *Kepler* (1.4 $M_\odot$). This agrees with the mass distribution found by Stello et al. (2016b) for stars with low-amplitude dipole modes.

Evolutionary stage. Mosser et al. (2012a) have reported the identification of low visibilities for stars on the RGB. Here, we report that stars with depressed mixed modes appear at any evolutionary stages. We identified depressed modes in secondary-clump stars, located on the same low-visibility branch as RGB stars (Fig. 3a). Owing to the mass dependence of the low-visibility stars, depressed modes are in fact over-represented in the secondary red clump. The situation is less clear for clump stars, since the low-visibility branch joins the group of normal visibility stars when $\Delta\nu \leq 4.5\,\mu$Hz. We however notice an over-abundance of red-clump stars with low visibilities; such stars are much more abundant than stars with visibilities above the normal value. An example of such a star is given in Fig. 2 (bottom panel).

Radial mode widths. Radial mode widths Γ_0, defined as full widths as half maximum, were measured following the method used by Vrard et al. (2015). Results are shown in Fig. 3b and summarized in Table 1. They are fully consistent with previous work obtained with CoRoT and *Kepler* (Baudin et al. 2011; Corsaro et al. 2012, 2015) and show a clear dependence with the evolutionary stage and stellar mass, as will be discussed in a forthcoming paper. In the clumps, Γ_0 of stars with depressed mixed modes behave as for the other stars. On the RGB, these stars appear to have slightly larger Γ_0 than the mean trend. This is however a mass effect only; Γ_0 increases with increasing masses and low visibility stars show higher mass (Stello et al. 2016b).

Asymptotic period spacing. Asymptotic period spacings follow the typical distribution identified in previous works (Mosser et al. 2012c, 2014; Vrard et al. 2016). We could not identify any departure to the distribution of the $\Delta\nu$–$\Delta\Pi_1$ relation (Fig. 3c). On the RGB, stars with depressed mixed modes show slightly lower values of $\Delta\Pi_1$ than the mean case, in agreement with their mass distribution (Vrard et al. 2016). Values are normal in the red clump. The large mass range and the non-degenerate conditions for helium ignition of secondary red clump stars explains the spread in the distribution of their seismic parameters, so that the spread for stars with depressed modes does not allow us to draw any conclusions.

Coupling factors. Coupling factors q were measured by Mosser et al. (in prep.) for about 4000 stars among the data set analyzed by Vrard et al. (2016). These factors are derived from the optimization of the method introduced by Mosser et al. (2015) for analyzing mixed modes. Results are shown in Fig. 3d, where stars with a low dipole-mode visibility are identified. Mosser et al. (in prep.) provide a discussion of the general trends observed in q as a function of the evolutionary stage. Here, we note that stars with depressed modes behave as the other stars. This suggests that the extent of the evanescent region between the pressure and gravity components is not impacted by the mechanism responsible for the amplitude mitigation, so that it is very similar as for normal stars (Unno et al. 1989; Takata 2016a).

Rotation. Fitting rotation requires a high signal-to-noise ratio in the oscillation spectrum, so that the difficulty of this measurement explains the limited number of stars with a complete fit. It is evidently a bias due to low visibilities. For the same reason, more fits than expected are obtained for the mixed-mode patterns of stars nearly seen pole-on, which are simpler than the general case since the rotational multiplets are reduced to the zonal modes (with an azimuthal order $m = 0$). In such cases,

Table 1. Mean mode width and lifetime (defined as the e-folding time of the mode energy), depending on the evolutionary, for red giants.

Evolutionary status	$\Delta\nu$ (μHz)	Γ_0 (nHz)	τ_0 (day)
RGB	15	118 ± 25	15.5 ± 3.3
RGB	10	121 ± 23	15.1 ± 3.0
RGB	6	118 ± 30	15.6 ± 3.9
Red clump	4	145 ± 37	12.6 ± 3.2
Secondary clump	7	178 ± 45	10.3 ± 2.6

the core rotation remains undetermined. When measured, rotational splittings show the typical distributions defined for red giants (Mosser et al. 2012b; Deheuvels et al. 2014, 2015).

3.3. Prevalence of depressed mixed modes

As the number of stars where the mixed-mode pattern can be fitted is limited, we checked whether the properties they display are verified by other stars.

3.3.1. Depressed modes versus pure pressure modes

A large number of oscillation spectra show peaks with a height much above eight times the background levels. Even in the case of low signal-to-noise ratio oscillation spectra, such peaks cannot all be created by noise. When their identification with radial, quadrupole, or octupole modes is excluded, we must conclude that depressed dipole mixed modes are obviously present in the whole spectrum. An example of such a star is given in Fig. 1b. When smoothed, oscillation spectra of such stars exhibit the typical mixed-mode pattern (Fig. 5).

In other cases, mixed modes are not apparent or cannot be distinguished from the noise (Fig. 1c). The identification of dipole mixed modes then requires different tools than those used earlier in this paper. In principle, the energy of the dipole modes peaks at the expected position of pressure dominated modes if modes are not mixed, but can be shifted by mode coupling. Hence, measuring this shift provides a way to identify whether modes are mixed or not. The measurement of the position of the dipole modes has to fight against the acoustic glitch (Vrard et al. 2015), the noise induced by background contribution, and the intrinsic shift due to finite lifetimes. We identified bright stars with high quality spectra on the low RGB, where the conditions of measurement are made easier (Fig. 1c). The shift of the actual position of the dipole modes with respect to the asymptotic expansion is shown in Fig. 6, together with the position shifts of radial, quadrupole, and octupole modes. The curves for these modes are remarkably close to each other, even for $\ell = 3$ modes, whereas dipole modes show a modulation as large as $\pm 0.04\,\Delta\nu$.

Synthetic tests were performed to evaluate the noise contribution. We reproduced typical conditions of observation and measured the location of pure pressure dipole modes. In the conservative case of a dipole mode width that is five times larger than the radial mode width, which is, in turn, much larger than the dipole width observed in other stars, shifts were less than $0.01\ \Delta\nu$ away of their expected position. The example shown in Fig. 6 is representative of any spectrum with a high enough signal-to-noise ratio. From this study, we conclude that depressed dipole mixed modes are not an exception, but evidently the rule. Very low visibilities cannot be associated exclusively with the full suppression of the oscillation in the core.

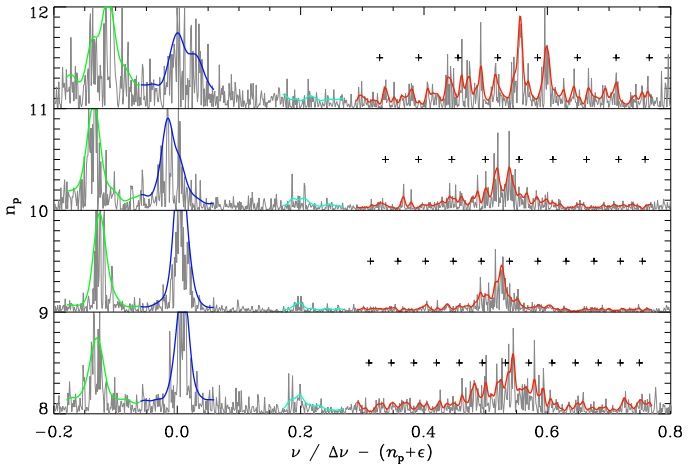

Fig. 5. Échelle spectrum of the RGB star KIC 9711269. Colored lines, with the same color code as in Fig. 1, emphasize the structure of the modes. Plus symbols approximately indicate the period spacings derived from the asymptotic expansion; the fit of the mixed modes, which would imply the fit of the rotational splittings, is however not possible.

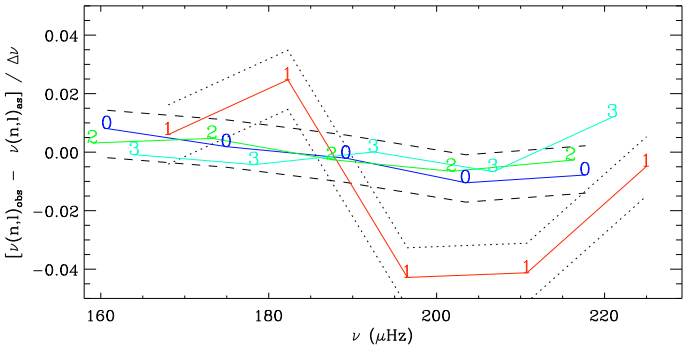

Fig. 6. Evidence of dipole mixed modes provided by the position of low-degree modes, with respect to the second-order asymptotic expansion of pure pressure modes, for the red giant 5810513 observed by *Kepler* (Fig. 1 bottom). The shifts are expressed in $\Delta\nu$ units. The dashed lines indicate the region where pure pressure low-degree modes are expected; the dotted lines provide uncertainties for the positions of the dipole modes.

3.3.2. Asymptotic period spacings

Asymptotic period spacings can be measured independent of the identification of the mixed-mode pattern (Vrard et al. 2016). Since measurements are difficult when dipole modes are depressed, we focused this study on all RGB stars with a magnitude brighter than $m_V = 11$, and performed an individual analysis of each oscillation spectra. These individual studies provided us with the measurement of the asymptotic period spacings in more than 90% of the cases. As a by-product, this study also confirmed that the structure of the excess power near the pressure-dominated mixed modes cannot result from the simple broadening of a single dipole pressure mode. This study fully confirmed that asymptotic period spacings of stars with depressed mixed modes are normal.

3.4. Summary of the observations: depressed modes are mixed

From the observations, we have derived that depressed modes are mixed and that their seismic properties, including their asymptotic period spacings, are normal.

- This information was directly obtained for the 71 red giants where the signal-to-noise ratio is high enough to fit the mixed-mode spectrum.
- For 96 stars, we measured the individual values of the coupling factors and of the period spacings. Again, these seismic values are normal. These 96 stars are considered in Sect. 4.
- At very low visibility, estimating the asymptotic period spacing is impossible. However, we showed that the dipole modes are shifted with respect to the expected position of pure pressure modes.
- The previous cases represent a small fraction of the 1109 stars with low amplitudes, but we showed that more than 90% of the stars with depressed modes brighter than $m_V = 11$ on the RGB have a mixed-mode pattern with a normal period spacing. This prevalence can be extrapolated to fainter stars since we do not expect any bias with magnitude. The situation for clump stars is comparable.

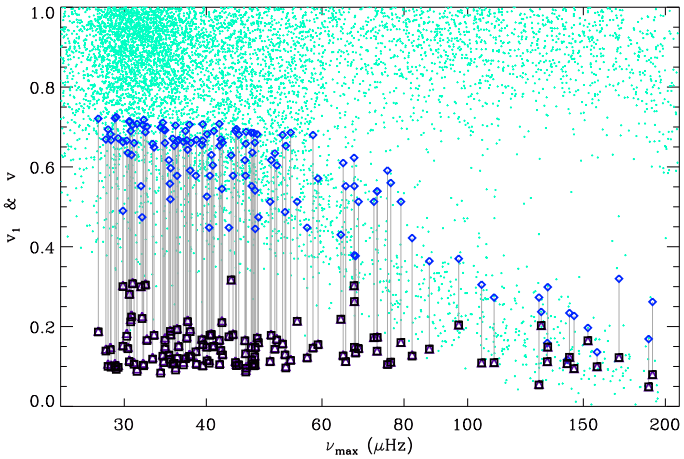

Fig. 7. Observed visibilities v_1 for the *Kepler* public data set of red giants, as a function of ν_{max}. Values for stars showing depressed mixed modes are emphasized with large diamonds and compared to the computed visibilities: large dark triangles for the low-coupling case (Eq. (16), as in Unno et al. 1989; Fuller et al. 2015) are very close to black squares for the strong-coupling case (Eq. (20)). Gray lines connect the observed and modeled values.

4. Observed versus predicted visibilities

As shown above, the observation of many red giants with depressed mixed modes invalidates the hypothesis of full suppression of the oscillation in the core for explaining low visibilities. This opens questions on the validity of Eq. (13) to explain the low visibility. Hence, we need to check whether the prediction of Eq. (13) is sustained. As our analysis is based on observations, we aim to check Eq. (13) through Eq. (20). Therefore, we first justify the validity of using Eq. (20), then test various hypotheses introduced by Fuller et al. (2015) to explain low visibilities.

4.1. Global seismic parameters

Using Eq. (20) for testing the observed visibilities requires information on the coupling factors q and on the radial mode widths Γ_0. The set of red giants with a low visibility, and for which all parameters of Eq. (20) are measured, is composed of 96 stars. We assumed that the mechanism responsible for the extra damping does not modify the stellar interior structure, so that q is representative of the transmission T. This assumption is theoretically justified by the analysis that is presented in Takata (2016b) and is observationally verified: as seen above, all stars have similar q and similar Γ_0, regardless of their visibility (Figs. 3b and d). In that respect, the stars with depressed mixed modes provide us indirectly with relevant tests and Eq. (20) can be used to test Eq. (13).

4.2. A significant disagreement

Assuming that q measured from mixed modes can replace the T value (Eq. (19)) and using observed Γ_0, we were able to compare the relation between the reduced observed visibilities v_1 and the calculated depressed visibility v predicted by Eq. (20). Contrary to previous work, the estimated visibilities do not match the observed visibilities, where modeled values are significantly smaller than the observed values (Fig. 7). We stress that the discrepancy is not due to the use of the formalism correct for strong coupling introduced by Takata (2016a,b). In fact, the difference is as high as a factor of 4 for the term $\tau_0\, T^2$ of Eq. (13). Relative uncertainties on q and Γ_0 cannot explain such a high difference. However, the disagreement is consistent with partial suppression of the oscillation in the core since observed visibilities are larger than modeled values. This evidence is ascertained by the fact that, as made clear by Fig. 7, not only stars with depressed mixed modes have observed visibilities that are much larger than predicted by the model. The discrepancy certainly indicates that previous analysis were based on inappropriate estimates of T.

5. Discussion

5.1. Depressed modes are mixed

Important facts were inferred from the observations presented in the previous sections: first, depressed modes are identified as mixed modes for all stars observed with a sufficient signal-to-noise ratio; second, period spacings of stars with depressed modes resemble normal period spacings; and third, core rotation rates also follow the normal distribution. We consider these three pieces of information next.

5.1.1. Depressed mixed modes

Mixed modes were directly or indirectly observed in many stars showing low visibilities. As already stated, the hypothesis of full suppression of the oscillation in the core is invalidated, since mixed modes result from the coupling of pressure waves in the envelope and gravity waves in the core. This observational result breaks the statement that the observation of low visibilities implies the suppression of the oscillation in the core. A mechanism able to damp the oscillation only partially is needed for explaining the low visibilities.

As a result, the mechanism proposed by Fuller et al. (2015) is not fully adequate since it relies on the total suppression of the dipole modes in the core. Furthermore, the equivalence between low visibility and magnetic greenhouse effect accepted

in follow-up papers (Cantiello et al. 2016; Stello et al. 2016b) is questionable.

5.1.2. Period spacings of depressed mixed modes

The measurement of normal period spacings in stars with depressed modes allows us to derive further information, since such spacings imply that the resonant cavity of gravity modes is not perturbed by the suppression mechanism. The mechanism responsible for the damping cannot modify the Brunt-Väisälä cavity at the high level of precision reached with seismology.

In that respect, the scattering process associated with the magnetic greenhouse effect is invalidated since it would modify the resonance condition of dipole modes with a smaller resonant cavity for the gravity waves (Fig. 1 of Fuller et al. 2015) and, hence, larger period spacings. Larger period spacings are not observed for depressed mixed modes. This proves that the magnetic greenhouse effect cannot explain the many cases where depressed mixed modes are observed. This mechanism may work in some other cases, but proving it then requires more information than simply having the visibilities of dipole modes. In any case, at this stage, the magnetic greenhouse effect cannot be a general solution for explaining depressed modes, and it is impossible to conclude the identity of the mechanism able to lower the dipole mode amplitude.

5.1.3. Rotational splittings of depressed mixed modes

The identification of the normal rotational splittings in stars with depressed modes provides us with similar conclusions. If there were a strong magnetic field in the cores of the stars with depressed modes, then Cantiello et al. (2016) predict that an extra magnetic splitting, which is comparable to the gravity mode period spacing in RGB stars, would be observed. As the core rotation rates inferred from the mixed-mode pattern follow a similar distribution to the reference set of stars, we can rule out the presence of the extra, magnetic splitting.

5.2. From individual visibilities to extra damping

The study of the widths of dipole mixed modes can provide promising information on the way amplitude are distributed in mixed modes. We illustrate this potential with the comparison of two twin stars with very close $\Delta\nu$ and $\Delta\Pi_1$. The star with normal visibility is used as a reference for the other with depressed modes. The resemblance of their mixed-mode pattern allowed us to compare their individual visibilities v_{n_m} (Fig. 8). The simplifications introduced either for normal stars (Sect. 2.2) or in the extreme case of full suppression of the oscillation in the core (Sect. 2.3) do not hold any more for the star with depressed modes. We have to rewrite Eq. (4) in case of an extra damping. For radial modes, we have

$$\Gamma_0 I_0 = -\frac{1}{\omega_0}\oint \delta W_0, \tag{23}$$

where ω_0 is the radial frequency and the cyclic integral represents the work during one radial oscillation. For a mixed mode, we have an extra damping, so that

$$\Gamma_{n_m} I_{n_m} = -\frac{1}{\omega_{n_m}}\oint \delta W_{n_m} \simeq -\frac{1}{\omega_{n_m}}\oint (\delta W_0 + \delta W_{\rm extra}), \tag{24}$$

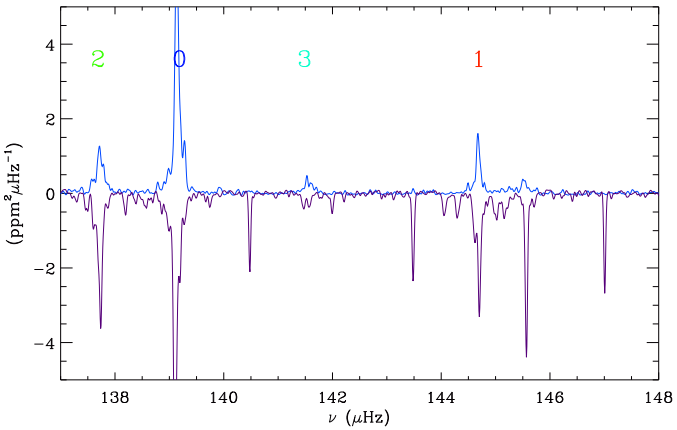

Fig. 8. Comparison of the smoothed spectra of two stellar twins, KIC 5295898 (with depressed modes; blue curve) and KIC 2157650 (with normal modes, nearly seen pole on; purple curve printed upside down). The width of the smoothing filter is 0.05 μHz, which is much smaller than the expected width of dipole modes if not mixed. A small shift in frequency is needed to superimpose the peaks.

assuming that the normal dipole work is similar to the radial work, except for the extra damping (e.g., Dupret et al. 2009; Benomar et al. 2014; Grosjean et al. 2014). Since radial and non-radial frequencies are close to each other, we have

$$\Gamma_{n_m} I_{n_m} = \Gamma_0 I_0 (1 + x), \tag{25}$$

with a similar definition for x as in Eq. (10); x represents the relative contribution of the extra damping.

From Eq. (4), we obtain a new expression for the mixed mode visibility,

$$v_{n_m} \simeq \frac{I_0}{(1+x)\, I_{n_m}} \simeq \frac{\Gamma_{n_m}}{(1+x)^2\, \Gamma_0}, \tag{26}$$

which demonstrates the capability of mixed modes to measure the relative extra damping x.

If we simply assume that x has limited variation in frequency, the total contribution v of the individual visibilities provides an estimate of the extra damping,

$$x \simeq \frac{1-v}{v}. \tag{27}$$

According to this relation, the magnitude of this relative extra-damping significantly decreases with stellar evolution. Very low visibilities observed for stars on the low RGB are due to a large absorption ($x \simeq 9$ when $v_1 = 0.1$), but $x \simeq 0.7$ only when $v_1 = 0.6$. For KIC 5295898 shown in Fig. 8, $x \simeq 2.6$.

5.3. No man's land

For completeness, we fitted the stars in the no man's land between normal and low-visibility stars (Figs. 3a and 7). We checked that these stars behave as other stars with similar seismic parameters. The presence of such stars is crucial for at least two reasons. First, they show that intermediate values between normal and low visibilities are possible. Second, those stars represent the intermediate case between normal and low visibility. This reinforces the fact that stars in which depressed mixed modes could be fully characterized are representative of all stars with low-amplitude dipole modes.

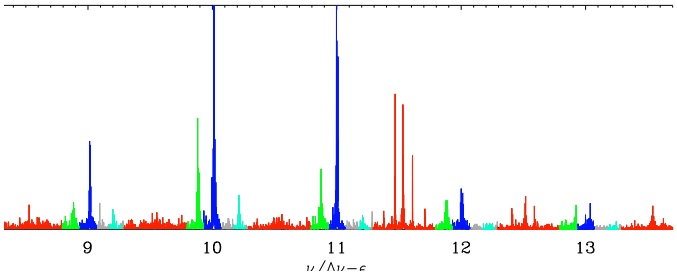

Fig. 9. Spectrum of the RGB star KIC 6975038 showing a strong gradient of the dipole mode amplitudes. Dipole modes have very low amplitudes below the radial order 11 and normal amplitudes above.

5.4. Visibility gradient

Three stars of our data set exhibit a clear visibility gradient: KIC 6975038 (Fig. 9), 7746983, and 8561221.

- The case of KIC 6975038 is investigated in Mosser et al. (in prep.). This star shows atypical seismic parameters: $\Delta\Pi_1$ is very low and q is unusually large compared to the general trend on the RGB (Mosser et al. 2015; Vrard et al. 2016). This star deserves a precise modeling beyond the scope of this work.
- KIC 8561221 was identified by García et al. (2014) as the least evolved observed star with depressed dipole modes among red giants observed with *Kepler*. It shows a very low dipole-mode visibility (Table A.1). However, mixed modes can be firmly identified. The asymptotic period spacing $\Delta\Pi_1 \simeq 114.8$ s is typical for $\Delta\nu \simeq 29.8\,\mu$Hz, but the core rotation of this star seems very high. We measure a core rotation rate of about $2.6\,\mu$Hz in contradiction with the values extracted from $\ell = 2$ and $\ell = 3$ modes by García et al. (2014).
- Compared to the two previous stars, the seismic parameters of KIC 7746983 are close to the values obtained on the RGB; only the dipole mode visibility is atypical. This gradient appears to be helpful for characterizing the mixed mode pattern; after KIC 8561221, this star is the second least evolved in our data set with low-dipole visibility.

The change of visibility with frequency was used by Fuller et al. (2015) as a further argument in favor of a large magnetic field for explaining the suppression of the oscillation, since the variation of the visibility with frequency matches their prediction. A more conservative analysis consists in remarking that the physics of oscillation damping has to be frequency dependent. Red giants showing a gradient of dipole visibility are certainly useful benchmark stars for understanding the nature and physics of the extra damping of the oscillation.

6. Conclusion

We performed a thorough study of red giants showing low dipole-mode visibility, based on the identification of their dipole mode pattern and the characterization of their global seismic properties. We have shown that these stars share the same global seismic parameters as other stars, regardless of the value of the dipole mode visibilities. This analysis sustains the fact that the mechanism responsible for the damping does not significantly impact the stellar structure and does not change the property of the cavity where gravity waves propagate.

We were able to determine that dipole depressed modes are mixed, even at very low visibilities. The existence of these depressed mixed modes implies that oscillations cannot be fully suppressed in the radiative core. Also, the observed visibilities are significantly higher than predicted from the modeling assuming full suppression in the core, which is consistent with partial suppression of the core oscillation only. Furthermore, the observations of normal period spacings in stars with depressed mixed modes indicate that the radiative core of these stars is not affected by the suppression mechanism.

These precise seismic signatures indicate that the magnetic greenhouse effect cannot explain the observed low visibilities of dipole modes (Fuller et al. 2015). This effect supposes the full suppression of the oscillation, which is discarded by the fact that depressed modes are mixed. Even if the mechanism could work with partial suppression only, the scattering process induced by the magnetic field in the radiative core is dismissed by the observation of the period spacings. As a result, inferring high magnetic fields in red giant from low visibilities (Stello et al. 2016b; Cantiello et al. 2016) is at least premature. This conclusion applies in the vast majority of stars that show low visibilities.

The low integrated visibilities reflect an extra mode damping but, at this stage, carry no direct information on the nature of this damping. Another damping mechanism must be found. This mechanism, which partially damps the dipole mixed modes, could be characterized by the measurement of the mixed mode widths.

Acknowledgements. We acknowledge the entire *Kepler* team, whose efforts made these results possible. B.M. thanks Jim Fuller for interesting discussions. B.M., K.B., C.P., C.B., M.J.G., and R.S. acknowledge financial support from the Programme National de Physique Stellaire (CNRS/INSU), from the French space agency CNES, and from the ANR program IDEE Interaction Des Étoiles et des Exoplanètes. M.T. is partially supported by JSPS KAKENHI Grant Number 26400219. M.V. acknowledges funding by the Portuguese Science foundation through the grant CIAAUP-03/2016-BPD, in the context of the project FIS/04434, co-funded by FEDER through the program COMPETE.

References

Ballot, J., Barban, C., & van't Veer-Menneret, C. 2011, A&A, 531, A124
Baudin, F., Barban, C., Belkacem, K., et al. 2011, A&A, 529, A84
Beck, P. G., Montalban, J., Kallinger, T., et al. 2012, Nature, 481, 55
Bedding, T. R., Mosser, B., Huber, D., et al. 2011, Nature, 471, 608
Belkacem, K., Samadi, R., Goupil, M.-J., & Dupret, M.-A. 2008, A&A, 478, 163
Belkacem, K., Marques, J. P., Goupil, M. J., et al. 2015, A&A, 579, A31
Benomar, O., Belkacem, K., Bedding, T. R., et al. 2014, ApJ, 781, L29
Cantiello, M., Fuller, J., & Bildsten, L. 2016, ApJ, 824, 14
Chaplin, W. J., Kjeldsen, H., Christensen-Dalsgaard, J., et al. 2011, Science, 332, 213
Corsaro, E., Stello, D., Huber, D., et al. 2012, ApJ, 757, 190
Corsaro, E., De Ridder, J., & García, R. A. 2015, A&A, 579, A83
Deheuvels, S., García, R. A., Chaplin, W. J., et al. 2012, ApJ, 756, 19
Deheuvels, S., Doğan, G., Goupil, M. J., et al. 2014, A&A, 564, A27
Deheuvels, S., Ballot, J., Beck, P. G., et al. 2015, A&A, 580, A96
De Ridder, J., Barban, C., Baudin, F., et al. 2009, Nature, 459, 398
Dupret, M., Belkacem, K., Samadi, R., et al. 2009, A&A, 506, 57
Dziembowski, W. A. 2012, A&A, 539, A83
Epstein, C. R., Elsworth, Y. P., Johnson, J. A., et al. 2014, ApJ, 785, L28
Fuller, J., Cantiello, M., Stello, D., Garcia, R. A., & Bildsten, L. 2015, Science, 350, 423
García, R. A., Pérez Hernández, F., Benomar, O., et al. 2014, A&A, 563, A84
Gaulme, P., Jackiewicz, J., Appourchaux, T., & Mosser, B. 2014, ApJ, 785, 5
Goupil, M. J., Mosser, B., Marques, J. P., et al. 2013, A&A, 549, A75
Grosjean, M., Dupret, M.-A., Belkacem, K., et al. 2014, A&A, 572, A11
Huber, D., Silva Aguirre, V., Matthews, J. M., et al. 2014, ApJS, 211, 2
Kallinger, T., Mosser, B., Hekker, S., et al. 2010, A&A, 522, A1

Kallinger, T., Hekker, S., Mosser, B., et al. 2012, A&A, 541, A51
Lagarde, N., Bossini, D., Miglio, A., Vrard, M., & Mosser, B. 2016, MNRAS, 457, L59
Mathur, S., Hekker, S., Trampedach, R., et al. 2011, ApJ, 741, 119
Michel, E., Baglin, A., Auvergne, M., et al. 2008, Science, 322, 558
Miglio, A., Montalbán, J., Baudin, F., et al. 2009, A&A, 503, L21
Montalbán, J., & Noels, A. 2013, in Eur. Phys. J. Web of Conf., 43, 3002
Mosser, B. 2015, EAS Pub. Ser., 73, 3
Mosser, B., & Miglio, A. 2016, in the CoRoT Legacy Book, ed. the CoRoT Team, Coordination A. Baglin (France: EDP Sciences), 197
Mosser, B., Belkacem, K., Goupil, M., et al. 2010, A&A, 517, A22
Mosser, B., Barban, C., Montalbán, J., et al. 2011, A&A, 532, A86
Mosser, B., Elsworth, Y., Hekker, S., et al. 2012a, A&A, 537, A30
Mosser, B., Goupil, M. J., Belkacem, K., et al. 2012b, A&A, 548, A10
Mosser, B., Goupil, M. J., Belkacem, K., et al. 2012c, A&A, 540, A143
Mosser, B., Michel, E., Belkacem, K., et al. 2013, A&A, 550, A126
Mosser, B., Benomar, O., Belkacem, K., et al. 2014, A&A, 572, L5
Mosser, B., Vrard, M., Belkacem, K., Deheuvels, S., & Goupil, M. J. 2015, A&A, 584, A50
Samadi, R., Belkacem, K., & Sonoi, T. 2015, in EAS Publ. Ser., 73, 111
Stello, D., Chaplin, W. J., Basu, S., Elsworth, Y., & Bedding, T. R. 2009, MNRAS, 400, L80
Stello, D., Cantiello, M., Fuller, J., Garcia, R. A., & Huber, D. 2016a, PASA, 33, e011
Stello, D., Cantiello, M., Fuller, J., et al. 2016b, Nature, 529, 364
Takata, M. 2016a, PASJ, 68, 109
Takata, M. 2016b, PASJ, 68, 91
Unno, W., Osaki, Y., Ando, H., Saio, H., & Shibahashi, H. 1989, in Nonradial oscillations of stars, eds. W., Unno, Y., Osaki, H., Ando, H., Saio, & H., Shibahashi
Vrard, M., Mosser, B., Barban, C., et al. 2015, A&A, 579, A84
Vrard, M., Mosser, B., & Samadi, R. 2016, A&A, 588, A87

Appendix A: Additional table

Table A.1. Seismic properties of 71 stars showing depressed mixed modes.

KIC	Evolutionary stage (1)	ν_{max} (μHz)	$\Delta\nu$ (μHz)	$\Delta\Pi_1$ (s)	q (2)	M ($M_\odot$)	Γ_0 (μHz) (3)	$\delta\nu_{rot}$ (nHz) (4)	v_1	v Low	v Strong
2573092	RC	35.3	4.08	293.8	0.24	1.48	0.14	35	0.60	0.181	0.178
2858129	RC2	40.5	4.22	320.9	0.26	1.93	0.16	80	0.58	0.181	0.178
2992350	RC	45.9	4.72	242.8	0.26	1.59	0.12	35	0.58	0.134	0.132
3443483	RGB	132.2	10.71	71.8	0.15	1.71	0.13	230	0.16	0.113	0.112
3532734	RGB	145.2	11.83	75.3	0.12	1.63	0.09	0	0.23	0.095	0.095
3660245	RC	33.3	4.22	297.0	0.25	1.19	0.15	35	0.65	0.181	0.178
3758505	RGB	157.4	12.06	80.6	0.15	1.84	0.13	500	0.14	0.100	0.099
4180939	RC2	65.2	5.80	241.0	0.24	2.29	0.11	50	0.55	0.114	0.112
4587050	RGB	191.2	14.47	73.8	0.10	1.60	0.08	530	0.26	0.080	0.080
4761301	RC	30.8	4.49	338.3	0.30	0.76	0.25	65	0.63	0.229	0.224
4772722	RC	37.3	4.30	310.0	0.31	1.42	0.18	38	0.67	0.175	0.170
5007332	RGB	96.9	8.44	68.7	0.10	1.76	0.14	310	0.37	0.204	0.204
5179471	RC2	47.0	4.56	256.0	0.28	2.17	0.10	110	0.64	0.109	0.106
5295898	RGB	142.9	11.39	75.3	0.10	1.72	0.10	210	0.23	0.123	0.123
5306667	RC	39.5	4.28	268.0	0.28	1.77	0.14	25	0.67	0.158	0.154
5339823	RC	40.4	4.28	317.2	0.45	1.76	0.16	80	0.45	0.115	0.108
5620720	RC2	57.0	5.35	264.7	0.29	2.14	0.14	45	0.45	0.124	0.121
5881079	RGB	67.2	6.14	68.3	0.10	1.96	0.17	0	0.62	0.303	0.302
5949964	RC	37.8	4.29	316.3	0.35	1.50	0.23	40	0.59	0.194	0.187
6037858	RC	43.3	4.57	244.4	0.25	1.76	0.16	50	0.45	0.178	0.174
6130770	RC	35.1	4.13	322.9	0.30	1.48	0.12	40	0.62	0.132	0.128
6210264	RC	40.7	4.78	290.0	0.25	1.60	0.17	60	0.63	0.183	0.180
6232858	RC2	50.0	4.90	235.8	0.28	1.87	0.11	55	0.51	0.115	0.112
6610354	RC2	46.9	4.57	209.3	0.28	2.44	0.11	65	0.55	0.119	0.116
6975038	RGB	128.4	10.61	57.9	0.35	1.44	0.14	280	0.27	0.056	0.054
7512378	RC	32.5	3.84	310.0	0.32	1.34	0.16	45	0.70	0.170	0.165
7515137	RGB	67.2	6.75	61.1	0.12	1.32	0.09	0	0.55	0.149	0.148
7693833	RGB	31.8	4.02	56.6	0.10	1.05	0.11	0	0.55	0.301	0.300
7746983	RGB	188.6	14.74	83.3	0.18	1.40	0.09	190	0.17	0.050	0.049
8009582	RC	35.2	4.21	282.4	0.22	1.36	0.08	30	0.56	0.120	0.118
8025383	RC	36.1	4.14	313.5	0.25	1.41	0.16	25	0.58	0.195	0.192
8283646	RGB	67.2	6.15	66.5	0.10	1.93	0.14	100	0.38	0.263	0.263
8391175	RGB	87.4	7.77	69.0	0.12	1.72	0.10	0	0.36	0.144	0.144
8396782	RC2	82.3	7.04	241.8	0.30	2.00	0.20	200	0.42	0.129	0.126
8432219	RC	42.3	4.59	283.2	0.30	1.66	0.24	45	0.55	0.215	0.210
8476202	RGB	109.7	9.42	71.7	0.12	1.57	0.09	0	0.27	0.110	0.110
8522050	RC2	75.5	6.72	188.1	0.30	2.06	0.16	60	0.59	0.108	0.105
8564277	RC	31.9	4.00	307.0	0.31	1.09	0.23	25	0.47	0.226	0.220
8564559	RC	45.8	4.70	240.9	0.25	1.79	0.15	40	0.62	0.167	0.164
8636174	RC2	43.9	4.51	305.7	0.25	2.00	0.16	35	0.58	0.182	0.179
8687248	RGB	170.0	13.10	77.8	0.12	1.59	0.14	0	0.32	0.123	0.122
8689599	RC	30.4	3.93	299.3	0.32	1.17	0.14	35	0.63	0.149	0.144
8771414	RC	38.6	4.23	274.0	0.25	1.82	0.11	28	0.58	0.139	0.137
8827934	RGB	55.0	5.37	63.8	0.15	1.80	0.14	0	0.51	0.214	0.213
9115334	RC2	67.5	6.09	179.2	0.30	2.00	0.19	220	0.38	0.137	0.134
9176207	RC2	59.2	5.41	314.6	0.24	1.96	0.15	100	0.57	0.157	0.154
9229592	RGB	72.0	6.85	67.2	0.15	1.62	0.14	230	0.51	0.173	0.172
9279486	RGB	132.4	10.89	76.8	0.12	1.59	0.15	200	0.30	0.149	0.149
9291830	RC2	47.5	4.41	261.8	0.30	2.50	0.15	70	0.44	0.151	0.147
9581849	RC	34.6	4.08	270.5	0.37	1.43	0.20	30	0.66	0.172	0.165
9650046	RC2	68.2	6.02	283.5	0.25	2.42	0.17	90	0.51	0.147	0.144
9711269	RGB	64.1	6.44	64.2	0.10	1.39	0.12	0	0.43	0.219	0.218
9719858	RC2	47.8	4.48	285.8	0.25	2.62	0.15	90	0.68	0.174	0.171
9947511	RC	30.7	3.75	349.5	0.33	1.35	0.22	30	0.69	0.218	0.212
10029821	RC2	64.6	5.90	259.3	0.29	2.08	0.16	50	0.61	0.129	0.126
10091729	RC2	72.8	6.34	295.3	0.23	2.18	0.20	60	0.54	0.175	0.173
10420655	RC	37.5	4.26	298.6	0.28	1.39	0.21	50	0.64	0.217	0.212
10422589	RC2	50.2	5.04	223.1	0.24	2.15	0.17	60	0.62	0.181	0.178
10469976	RC2	52.7	4.81	258.0	0.30	2.35	0.14	30	0.49	0.132	0.129
10528917	RGB	76.4	7.52	73.1	0.13	1.36	0.08	220	0.56	0.111	0.111
10653383	RC	40.1	4.42	248.5	0.26	1.60	0.13	30	0.53	0.151	0.148
10854564	RC	29.9	4.26	293.5	0.22	0.69	0.26	30	0.66	0.304	0.300
11413158	RC2	58.1	4.99	210.6	0.28	2.86	0.15	80	0.68	0.149	0.146
11462972	RC2	29.9	4.26	318.0	0.26	1.89	0.13	30	0.49	0.154	0.151
11519450	RGB	72.8	6.87	68.1	0.14	1.65	0.10	180	0.54	0.139	0.138
11598312	RC2	48.0	4.82	281.5	0.22	1.96	0.13	50	0.47	0.161	0.159
12058556	RGB	105.0	9.35	72.7	0.15	1.40	0.11	0	0.31	0.110	0.109
12070510	RC	35.3	4.06	304.9	0.23	1.36	0.14	50	0.52	0.191	0.188
12109388	RC	40.9	4.25	245.3	0.26	1.82	0.13	50	0.60	0.152	0.149
12453551	RC2	51.2	5.02	270.8	0.29	2.04	0.19	70	0.60	0.170	0.166
12691734	RC2	46.8	4.34	338.5	0.31	2.73	0.15	50	0.69	0.151	0.147

Notes. (1) RGB: red giant branch; RC: red clump; RC2: secondary red clump. (2) Uncertainties on q are of about ±0.027 for stars on the RGB and ±0.057 in the red clump. (3) Uncertainties on Γ_0 are of about 30%. (4) A null value for $\delta\nu_{rot}$ indicates that the rotational splitting could not be measured because the star is seen pole-on.